Energy levels and line intensities of Pr^{3+} in $LiYF_4$*

L. Esterowitz, F. J. Bartoli, and R. E. Allen
Naval Research Laboratory, Washington, D.C. 20375

D. E. Wortman, C. A. Morrison, and R. P. Leavitt
Harry Diamond Center, Adelphi, Maryland 20783

(Received 6 July 1978)

High-resolution polarized absorption and fluorescence spectra of Pr^{3+} in $LiYF_4$ were measured at temperatures between 10 and 300°K. Energy-level assignments were made assuming electric-dipole transition selection rules for S_4 site symmetry. Forty-six energy levels of the $4f^2$ ground configuration were established, including 44 in the lowest nine multiplets. Crystal-field parameters were determined that gave a rms deviation of 15.8 cm^{-1} between 41 of the experimental energy levels and calculated values. The parameters were $B_{20} = 488.9$, $B_{40} = -1043$, $B_{44} = 1242$, $B_{60} = -42$, Re $B_{64} = 1213$, and Im $B_{64} = 22.5$ cm^{-1}. These parameters were used to obtain the remaining energy levels, yielding a complete energy-level scheme for the $4f^2$ configuration of Pr^{3+}. The crystal-field parameters for Pr^{3+} in $LiYF_4$ were compared to those for other ions in this host. A theoretical calculation of line intensities was performed in which the odd-fold crystal-field parameters were obtained from a lattice sum. Line intensities were measured and compared with theory.

I. INTRODUCTION

In the present work a systematic spectroscopic investigation of trivalent praseodymium in lithium yttrium fluoride ($LiYF_4$) was undertaken. High-resolution polarized absorption and fluorescence spectra were measured at temperatures between 10 and 300°K and analyzed to determine the energy levels of the $4f^2$ ground configuration. Spectroscopic data previously reported for $LiYF_4$:Pr^{3+} have either been incomplete[1] or have led to incorrect[2] energy assignments. Experimental line intensities for Pr^{3+} in $LiYF_4$ were also determined and are reported for the first time. The spectra were analyzed in detail to obtain empirical parameters which describe the effects of the host lattice on the Pr^{3+} energy levels. In this analysis a complete energy-level scheme for the $4f^2$ ground configuration of Pr^{3+} was determined. Crystal-field parameters were obtained and compared with those for other rare-earth ions[3-6] in $LiYF_4$. A theoretical calculation of line intensities was performed in which the odd-fold crystal-field parameters were determined *a priori* from a lattice sum. Calculated intensities were compared with measured values in order to determine the limitations[7] of current crystal-field theory in predicting[8] accurately line intensities.

Interest in the Pr ion for laser applications has been heightened recently due to the 479-nm laser transition observed[9] in $LiYF_4$:Pr^{3+}. It was shown in that study that the blue-green laser transition in $LiYF_4$:Pr^{3+} terminates on the lowest level in the ground-state multiplet, indicating three-level laser operation. Since four-level laser action[10] is necessary to achieve high efficiency and low threshold, other hosts[11] where the laser transition terminates on an upper level of the ground multiplet are desired. Numerous experimental studies can be obviated if the energy levels and transition probabilities for the Pr^{3+} ion in any potential host can be reliably predicted. The adequacy of current theory for this purpose has not yet been assessed for Pr^{3+} in any host. The comparison between theory and experiment made in this work for $LiYF_4$:Pr^{3+} provides a useful test of the predictive capability of current crystal-field theory.

II. THEORY

A. Energy-level calculations

Free-ion wave functions were calculated by diagonalizing in a Russell-Saunders basis of J states a Hamiltonian containing the Coulomb, spin-orbit, L^2, $G(G_2)$, and $G(R_7)$ interactions.[12] The free-ion parameters chosen were those obtained[13] by Carnall, Fields, and Rajnak for praseodymium in aqueous solution:

$$E^1 = 4548.2, \quad E^2 = 21.937, \quad E^3 = 466.73,$$

$$\zeta = 740.8, \quad \alpha = 21.255, \quad \beta = -799.94, \quad \gamma = 1342.9,$$

(all in units cm^{-1}). Values of the Slater parameters[12] corresponding to those E^i values are (in units cm^{-1})

$$F_2 = 305.220, \quad F_4 = 46.2767, \quad F_6 = 4.434\,81. \quad (1)$$

Using this set of free-ion parameters, we cal-

culated reduced matrix elements of U^2, U^4, and U^6 between all of the intermediate-coupled wave functions representing the multiplets of the electronic ground configuration of the free ion. A separate program then selected the reduced matrix elements between the free-ion multiplets in a truncated basis (for the case of Pr^{3+}, all 13 multiplets), set up the crystal spaces for the given crystal-field symmetry (S_4 for the case of $LiYF_4$) and diagonalized in that space of multiplets the crystal-field Hamiltonian given by the expansion

$$H_3 = \sum_{i,k,q} B_{kq}^{\dagger} C_{kq}(i) , \tag{2}$$

where C_{kq} is a spherical tensor of rank k and projection q, and the B_{kq} are the crystal-field parameters which describe the effect of the crystal on the free-ion energy levels. The i sum is over the electrons of the $4f^2$ configuration. The S_4 point-group symmetry at the Y^{3+} sites in the crystal lattice limits the even-k parameters that can be nonzero to B_{20}, B_{40}, B_{60}, B_{44}, and B_{64}.[14] Although B_{44} and B_{64} can both be complex, one may choose a coordinate system where B_{44} is real and positive.

In making the above calculations, the centroids associated with the free-ion multiplets were introduced as parameters and were not chosen as the free-ion energies resulting from diagonalizing the free-ion Hamiltonian. In this way, the centroids were freely varied so that, together with the full diagonalization of the crystal-field Hamiltonian, a more exact fitting to experimental crystal energies was possible. The resultant centroids obtained in this manner reflect what "free-ion" centroids of the rare-earth ion would be observed in the crystal if the even components of the static crystal field were "turned off."

B. Intensity Calculations

Approximate intensity calculations were performed using the Judd-Ofelt[15,16] theory of induced electric dipole transitions. In a spherical basis, the α component of the induced electric dipole operator is given by[16]

$$p_\alpha = -2\sum_{lkt}\left(\frac{7(2l+1)}{3}\right)^{1/2}(2t+1)\,W(k133;tl)R_k(l) \times\langle l(0)1(0)\,|\,3(0)\rangle\langle 3(0)k(0)\,|\,l(0)\rangle \times[A^{(k)}U^{(t)}]_\alpha^{(1)} , \tag{3}$$

where

$$R_k(l) = \sum_n \int R(4f)R(nl)r^k\,dr \int \frac{R(4f)R(nl)r\,dr}{\Delta E_{nl}} . \tag{4}$$

In Eq. (3) above, the sum on l covers $l=2$ and $l=4$; the k sum is over $k=1,3,5,7$; and the t sum is over $t=2,4,6$. The quantities

$$\langle j_1(m_1)j_2(m_2)\,|\,J(M)\rangle$$

are Clebsch-Gordan coefficients, $W(k133;tl)$ is a Racah coefficient, and $A^{(k)}$ is a tensor whose components A_{kq} represent a spherical decomposition of the odd-parity part of the crystalline electric field in the vicinity of the rare-earth ion. The quantity $[A^{(k)}U^{(t)}]_\alpha^{(1)}$ represents the coupling of the tensors $A^{(k)}$ and $U^{(t)}$ to form a tensor of rank 1 and projection α via a Clebsch-Gordan coefficient. In Eq. (4), ΔE_{nl} is the difference in energy between the configuration $4f^{x-1}nl$ (or $nd^9 4f^{x+1}$) and the ground configuration $4f^x$ ($x=2$ for Pr^{3+}). The quantities $R(nl)$ are radial wave functions for the state (nl). For d electrons ($l=2$), the n sum runs over the configurations $3d^9 4f^{x+1}$ and $4d^9 4f^{x+1}$, as well as $4f^{x-1}$nd, $n \geq 5$. For g electrons the configurations $4f^{x-1}ng$, $n \geq 5$, are considered.

The line strength of a transition is defined[17]

$$S_{fi} = \sum_{f,i} |\langle f|\vec{p}|i\rangle|^2 , \tag{5}$$

where the sums over i,f are over the individual components of the levels i and f.

The integrated absorption coefficient is given by

$$\int \alpha(\nu)\,d\nu = \frac{e^2}{\hbar c}\,\frac{4\pi^2 c_0 \nu_0 \chi}{g_i}\sum_{f,i}|\langle f|\vec{\epsilon}\cdot\vec{p}\,|i\rangle|^2 , \tag{6}$$

where c_0 is the concentration of absorbers in ions/cm^3, g_i is the degeneracy of the initial state, $\vec{\epsilon}$ is a unit vector in the direction of polarization of the incoming wave, ν_0 is the center frequency of the transition, and $\chi = \frac{1}{9}n(n^2+2)^2$, where n is the index of refraction. The integrated absorption coefficient is related to the line strength. For π-polarized lines we have

$$\int \alpha(\nu)\,d\nu = \frac{e^2}{\hbar c}\,\frac{4\pi^2 c_0 \nu_0 \chi}{g_i} S_{fi} , \tag{7a}$$

and for σ polarized lines

$$\int \alpha(\nu)\,d\nu = \frac{e^2}{\hbar c}\,\frac{2\pi^2 c_0 \nu_0 \chi}{g_i} S_{fi} . \tag{7b}$$

The factor-of-2 difference between Eqs. (7a) and (7b) is due to the different angular distribution of the radiation for these polarizations. For a given ion the probability per unit time of spontaneous emission of a photon in a direction $\hat{k}$ with polarization $\vec{\epsilon}$ is given by

$$dP_{fi} = \frac{\nu_0^3 e^2 \chi}{(2\pi)^4 g_i c^3 \hbar}\sum_{f,i}|\langle f|\vec{\epsilon}\cdot\vec{p}\,|i\rangle|^2\,d\Omega_{\hat{k}} , \tag{8}$$

and is proportional to ν_0^2 times the integrated

absorption coefficient, with the same coefficient of proportionality for all transitions.

We have evaluated the line strengths for $LiYF_4:Pr^{3+}$ using the Judd-Ofelt approximation. The quantities $R_k(l)$ have been evaluated using the following assumptions.

(a) $R_k(d)$ is dominated by the $4f$-$5d$ transition. The configuration $4f^{x-1}5d$ is separated from $4f^x$ by ΔE_{5d}. We assume

$$\langle 4f|r^k|5d\rangle = (\tau')^{-k}\langle 4f|r^k|5d\rangle_{\mathrm{HF}},$$

$\tau' = 0.51$, to compute the $R_k(d)$ using Hartree-Fock (HF) wave functions.[18]

(b) $R_k(g)$ is evaluated assuming all $4f^{x-1}ng$ configurations are approximately degenerate at a separation ΔE_g from $4f^x$, using the closure property of the set $R(ng)$. We assume

$$\langle 4f|r^k|4f\rangle = \tau^{-k}\langle 4f|r^k|4f\rangle_{\mathrm{HF}},$$

with $\tau = 0.76$, to compute the $R_k(g)$ using HF wave functions.[19]

Using[20] $\Delta E_{5d} = 61\,200\ \mathrm{cm}^{-1}$ and $\Delta E_g = 238\,400\ \mathrm{cm}^{-1}$, we have arrived at the following set of $R_k(l)$ for Pr^{3+}:

$$R_1(d) = 3.324, \quad R_1(g) = 2.210,$$
$$R_3(d) = 6.839, \quad R_3(g) = 2.786,$$
$$R_5(d) = 22.98, \quad R_5(g) = 7.538,$$
$$R_7(g) = 36.35.$$

The units of $R_k(l)$ are $10^{-6}\ \text{Å}^{k+1}/\mathrm{cm}^{-1}$.

The crystal-field components A_{kq} have been computed using an effective point-charge model[4] with a charge of +3 on the yttrium ion, +1 on the lithium ion, and −1 on the fluorine ion. These give for the odd-k A_{kq} (rotated to a frame where A_{44} is real and positive):

$$A_{32} = 657 - 667i, \quad A_{52} = -2671 - 59i$$
$$A_{72} = 7 + 14i, \quad A_{76} = 254 + 45i.$$

The units of A_{kq} are $\mathrm{cm}^{-1}/\text{Å}^k$.

Computations of electric dipole transition probabilities were made using the full intermediate-coupling J-mixed wave functions.

C. Symmetry considerations

The eigenstates obtained in the above calculations transform[21] according to one of four irreducible representations (Γ_1, Γ_2, Γ_3, and Γ_4) of the S_4 point group. The levels characterized by wave functions transforming as Γ_3 and Γ_4 are degenerate and are designated $\Gamma_{3,4}$. The space is 91 dimensional and separates into a 25×25, a 24×24, and two 21×21 matrices. The first two, together with one of the latter, need to be diagonalized to determine, respectively, the energy levels for Γ_1, Γ_2, and $\Gamma_{3,4}$.

The classification of the experimental energy levels is made by analyzing the polarization data. According to the transformation properties of the electric dipole operator, identical axial and σ-polarized spectra (within a multiplicative factor) require the use of electric-dipole selection rules. Identical axial and π-polarized spectra require the use of magnetic dipole selection rules. A comparison of measured σ, π, and axial spectra for $LiYF_4:Pr^{3+}$ indicates that electric dipole transitions predominate.

In examining the spectra, we also considered selection rules[21] for D_{2d} point-group symmetry (S_4 is a subgroup of D_{2d}) since this may help to explain many of the low-intensity lines. If the Pr^{3+} ion were in a site of D_{2d} symmetry, certain transitions would be forbidden, as shown in Table I. If, however, the local site symmetry is perturbed by a lower-symmetry environment, such as S_4, some of the forbiddenness is lifted. In the energy-level calculations, the imaginary component of B_{64} ($\mathrm{Im}B_{64}$) is a certain measure of the difference between D_{2d} and S_4. The odd-fold B_{kq} (odd k), however, enter the intensity calculations, and even if $\mathrm{Im}B_{64} = 0$, the imaginary B_{kq} for odd k are not necessarily small in S_4; they are 0 in D_{2d}.[22] Since we have considered both S_4 and D_{2d}, we have listed the corresponding identifications of the S_4 levels in D_{2d} notation in Table II. The full rotation-group compatibility tables for S_4 and D_{2d} are given in Table III.

TABLE I. Electric-dipole selection rules[a] in S_4 and D_{2d}. This notation corresponds to that used by Koster *et al.*[b].

S_4	Γ_1	Γ_2	Γ_3	Γ_4
Γ_1	•••	π	σ	σ
Γ_2	π	•••	σ	σ
Γ_3	σ	σ	•••	π
Γ_4	σ	σ	π	•••

D_{2d}	Γ_1	Γ_2	Γ_3	Γ_4	Γ_5
Γ_1	•••	•••	•••	π	σ
Γ_2	•••	•••	π	•••	σ
Γ_3	•••	π	•••	•••	σ
Γ_4	π	•••	•••	•••	σ
Γ_5	σ	σ	σ	σ	π

[a] A coordinate system rotated by $\frac{1}{4}\pi$ about the z axis gave correct but different selection rules in Ref. 6.
[b] Reference 21.

TABLE II. Identifications of the irreducible representations of the D_{2d} point group in S_4 notation.

S_4	D_{2d}
Γ_1	Γ_1, Γ_2
Γ_2	Γ_3, Γ_4
$\Gamma_{3,4}$	Γ_5

TABLE III. Full rotation-group compatibility tables for the groups S_4 and D_{2d}. The irreducible representations in the parentheses in S_4 relate to those in parentheses in D_{2d}, and likewise for the square brackets.

	S_4	D_{2d}
D_0^+	Γ_1	Γ_1
D_1^+	$\Gamma_1 + (\Gamma_3+\Gamma_4)$	$\Gamma_2 + (\Gamma_5)$
D_2^+	$\Gamma_1 + 2[\Gamma_2] + (\Gamma_3+\Gamma_4)$	$\Gamma_1 + [\Gamma_3+\Gamma_4] + (\Gamma_5)$
D_3^+	$\Gamma_1 + 2[\Gamma_2] + 2(\Gamma_3+\Gamma_4)$	$\Gamma_2 + [\Gamma_3+\Gamma_4] + 2(\Gamma_5)$
D_4^+	$3\Gamma_1 + 2[\Gamma_2] + 2(\Gamma_3+\Gamma_4)$	$2\Gamma_1+\Gamma_2 + [\Gamma_3+\Gamma_4] + 2(\Gamma_5)$
D_5^+	$3\Gamma_1 + 2[\Gamma_2] + 3(\Gamma_3+\Gamma_4)$	$\Gamma_1 + 2\Gamma_2 + [\Gamma_3+\Gamma_4] + 3(\Gamma_5)$
D_6^+	$3\Gamma_1 + 4[\Gamma_2] + 3(\Gamma_3+\Gamma_4)$	$2\Gamma_1+\Gamma_2 + 2[\Gamma_3+\Gamma_4] + 3(\Gamma_5)$

III. EXPERIMENTAL PROCEDURE

Fluorescence and absorption measurements were obtained using a high-resolution 0.85-m Spex double monochromator for emission lines between 31 600 and 9650 cm^{-1}. For lower-energy fluorescence lines a 1-m McPherson spectrometer with interchangeable gratings was used. The Spex double monochromator employs a pair of 1200 grooves/mm gratings yielding a maximum resolution better than 0.2 cm^{-1}. The McPherson spectrometer was operated with 600 grooves/mm at a resolution better than 1 cm^{-1}. Signal detection above 12 000 cm^{-1} was accomplished by a RCA Model C31034A GaAs photomultiplier tube cooled to −30°C and photon-counting electronics. Below 12 000 cm^{-1} a RCA Model C30811 silicon avalanche photodiode was used. In the latter case the optical source was chopped and the detector signal measured by a PARC Model 124 lock-in amplifier with a Model 116 plug-in preamplifier.

The samples used in this investigation are high optical quality $LiYF_4$ crystals grown by MIT using a top-seeded-solution technique. The crystals were grown in a purified argon atmosphere from a nonstoichiometric melt containing YF_3 and a slight excess of LiF. The trivalent praseodymium ions enter substitutionally for Y^{3+}. The concentration of Pr^{3+} in the crystals studied is nominally 0.2 at.%. Samples were cut with two faces perpendicular to the c axis of the crystals and all faces were optically polished.

Crystal samples were mounted in an Air Products closed-cycle refrigerator capable of operating between 8 and 300°K. The temperature of the sample was regulated to within 0.1°K using a GaAs temperature sensing diode and a PARC Model 152 temperature controller.

Laser-excited fluorescence measurements were performed in which a focused laser beam is propagated perpendicular to both the axis of observation and the c axis of the $LiYF_4$:Pr^{3+} crystal. The 4765-Å line of a cw argon laser, polarized parallel to the c axis (π), was used to pump the crystal for $^3P_0$ fluorescence. For $^1D_2$ fluorescence measurements an argon-laser-pumped dye laser was employed to pump the $^1D_2$ level directly. The focused dye-laser beam was polarized perpendicular to the c axis (σ) and was tuned slightly above the 17 083-cm^{-1} σ absorption of the Pr^{3+} ion. This was done to achieve relatively uniform absorption and to avoid sample heating. At both laser wavelengths the laser power incident on the crystal was several hundred milliwatts. The greater sensitivity obtained by laser excitation permitted the observation of weak emission lines not found using incoherent sources.[2] Absorption measurements were made by illuminating the crystal perpendicular to the c axis with parallel light from a tungsten lamp. In both absorption and fluorescence experiments light from the sample was collected by a double lens system which produces parallel light between the lenses. Polarization selection was made by means of a Glan-Thompson polarizer. To compensate for the polarization sensitivity of the spectrometers, a $\lambda/2$ achromatic Fresnel rhomb retarder with a 25-mm clear aperture was placed in the parallel light between the lenses. This device rotates the polarization of the light by an arbitrary angle, and was used to rotate the polarization of the optical signals in such a way that both σ-polarized and π-polarized light enter the spectrometers with the same polarization. The wavelength readouts of the spectrometers were calibrated using the first and second order of Hg emission lines and of various lines of argon and HeNe lasers.

IV. EXPERIMENTAL RESULTS

Results of fluorescence and absorption measurements are summarized in Tables IV–VII for the $^3H_4$, $^3H_5$, $^3H_6$, $^3F_2$, $^3F_3$, $^3F_4$, $^1G_4$, $^1D_2$, $^3P_0$, and $^3P_2$ states. The tables present the line frequency *in vacuo*, the polarization and integrated intensity, S_4 symmetry assignment, and the derived energy levels for each multiplet. The spectra reported were obtained at 10, 30, and 80°K. The temperatures listed in the tables refer to the lowest of these three temperatures at which the transition was observed. The intensities reported for absorption refer to the absorptance $A = -\log_{10}(I_t/I_i)$, where I_t and I_i are the trans-

TABLE IV. Absorption of the $^3P_0$, $^1D_2$, and $^1G_4$ levels in $LiYF_4:Pr^{3+}$ at 10, 30, and 80 °K. The line energy in vacuum, polarization and relative intensity, S_4 symmetry assignment, and derived energy levels are given. The temperature indicated refers to the lowest of the three temperatures for which a line is observed.

Multiplet	ν_{vac} (cm^{-1})	Polarization	Temp. (°K)	S_4 symmetry assignment	ν_E (cm^{-1})
$^3P_0$	20 860	π	10	$\Gamma_2 \rightarrow \Gamma_1$	20 860
	20 781	σ	30	$\Gamma_{3,4} \rightarrow \Gamma_1$	20 860
$^1D_2$	16 661	3σ	30	$\Gamma_{3,4} \rightarrow \Gamma_2$	16 740
	16 731	8σ	30	$\Gamma_{3,4} \rightarrow \Gamma_1$	16 810
	16 810	1000π	10	$\Gamma_2 \rightarrow \Gamma_1$	16 810
	17 004 [a]	π	80	$\Gamma_{3,4} \rightarrow \Gamma_{3,4}$	17 083 [a]
	17 083 [a]	797σ [a]	10	$\Gamma_2 \rightarrow \Gamma_{3,4}$	17 083 [a]
	17 327	σ	80	$\Gamma_{3,4} \rightarrow \Gamma_2$	17 406
$^1G_4$	9 620	90σ	30	$\Gamma_{3,4} \rightarrow \Gamma_1$	9 699
	9 699	423π	10	$\Gamma_2 \rightarrow \Gamma_1$	9 699
	9 753	45π	30	$\Gamma_{3,4} \rightarrow \Gamma_{3,4}$	9 832
	9 832	733σ	10	$\Gamma_2 \rightarrow \Gamma_{3,4}$	9 832
	9 832	18π	10	$\Gamma_2 \rightarrow \Gamma_{3,4}$ (MD)	9 832
	10 112	1000σ	10	$\Gamma_2 \rightarrow \Gamma_{3,4}$	10 112
	10 217	10π	10	$\Gamma_2 \rightarrow \Gamma_1$	10 217
	10 313	41π	10	$\Gamma_2 \rightarrow \Gamma_1$	10 313

[a] Broad line (~100 cm^{-1}) with structure superimposed.

TABLE V. Observed $^3P_0$ fluorescence for $LiYF_4:Pr^{3+}$ at 10 °K. (Same quantities described in Table IV are given.)

Terminal multiplet	ν_{vac} (cm^{-1})	Polarization and relative intensities	S_4 symmetry assignment	ν_E (cm^{-1})
$^3H_4$	20 860	1000π	$\Gamma_1 \rightarrow \Gamma_2$	0
	20 781	249σ	$\Gamma_1 \rightarrow \Gamma_{3,4}$	79
	20 364	94σ	$\Gamma_1 \rightarrow \Gamma_{3,4}$	496
$^3H_5$	18 588	120σ	$\Gamma_1 \rightarrow \Gamma_{3,4}$	2 272
	18 580	20π	$\Gamma_1 \rightarrow \Gamma_2$	2 280
	18 519	81σ	$\Gamma_1 \rightarrow \Gamma_{3,4}$	2 341
	18 311	950π	$\Gamma_1 \rightarrow \Gamma_2$	2 549
	18 180–18 320 [a]	1000σ [a]	$\Gamma_1 \rightarrow \Gamma_{3,4}$	2 540–2 680
$^3H_6$	16 546	$>1000\pi$	$\Gamma_1 \rightarrow \Gamma_2$	4 314
	16 466	$>1000\sigma$	$\Gamma_1 \rightarrow \Gamma_{3,4}$	4 394
	16 406	675σ	$\Gamma_1 \rightarrow \Gamma_{3,4}$	4 454
	16 303 [b]	813π [b]	$\Gamma_1 \rightarrow \Gamma_2$	4 557 [b]
	15 953	198π	$\Gamma_1 \rightarrow \Gamma_{3,4}$	4 907
	15 915	37π	$\Gamma_1 \rightarrow \Gamma_2$	4 945
$^3F_2$	15 659	186π	$\Gamma_1 \rightarrow \Gamma_2$	5 201
	15 637	1000σ	$\Gamma_1 \rightarrow \Gamma_{3,4}$	5 221
	15 518	366π	$\Gamma_1 \rightarrow \Gamma_2$	5 342
$^3F_3$	14 379	17σ	$\Gamma_1 \rightarrow \Gamma_{3,4}$	6 481
	14 339	1000π	$\Gamma_1 \rightarrow \Gamma_2$	6 521
	14 189	2σ	$\Gamma_1 \rightarrow \Gamma_{3,4}$	6 671
	14 174	78π	$\Gamma_1 \rightarrow \Gamma_2$	6 686
$^3F_4$	13 918	8σ	$\Gamma_1 \rightarrow \Gamma_{3,4}$	6 942
	13 877	1000π	$\Gamma_1 \rightarrow \Gamma_2$	6 983
	13 718	2π	$\Gamma_1 \rightarrow \Gamma_{3,4}$	7 142
$^1G_4$	11 026	301σ	$\Gamma_1 \rightarrow \Gamma_{3,4}$	9 832
	10 930	1000π	$\Gamma_1 \rightarrow \Gamma_2$	9 930
	10 849	647π	$\Gamma_1 \rightarrow \Gamma_2$	10 011

[a] Very broad structured band.

[b] Line position and integrated intensity are uncertain because of vibronic structure in spectrum.

mitted and incident intensities, respectively. Only relative intensities are given for both absorption and fluorescence, the strongest line for each multiplet being normalized to 1000. Relative intensities between multiplets or between $^3P_0$ and $^1D_2$ fluorescence are not presented. Identifications of energy levels of Pr^{3+} in $LiYF_4$ are consistent with electric dipole selection

TABLE VI. Observed $^1D_2$ fluorescence for $LiYF_4$:Pr^{3+} at 10, 30, and 80 °K. (The same quantities described in Table IV are given.)

Terminal multiplet	ν_{vac} (cm^{-1})	Polarization and relative intensity	Temp. (°K)	S_4 symmetry assignment	ν_E (cm^{-1})
$^3H_4$	16 810	π	30	$\Gamma_1 \rightarrow \Gamma_2$	0
	16 740	5σ	10	$\Gamma_2 \rightarrow \Gamma_2$ (MD) [a]	0
	16 731	σ	30	$\Gamma_1 \rightarrow \Gamma_{3,4}$	79
	16 661	1000σ	10	$\Gamma_2 \rightarrow \Gamma_{3,4}$	79
	16 661	11π [b]	10	$\Gamma_2 \rightarrow \Gamma_{3,4}$ (MD)	79
	16 520	102π	10	$\Gamma_2 \rightarrow \Gamma_1$	220 [c]
	16 314	σ	80	$\Gamma_1 \rightarrow \Gamma_{3,4}$	496
	16 244	891σ	10	$\Gamma_2 \rightarrow \Gamma_{3,4}$	496
$^3H_5$	14 487	200π	10	$\Gamma_2 \rightarrow \Gamma_1$	2253
	14 468	1000σ	10	$\Gamma_2 \rightarrow \Gamma_{3,4}$	2272
	14 443	2π	10	$\Gamma_2 \rightarrow \Gamma_1$	2297
	14 399	55σ	10	$\Gamma_2 \rightarrow \Gamma_{3,4}$	2341
	14 075–14 205 [d]	1000π [d]	10	$\Gamma_2 \rightarrow \Gamma_1$	2535–2665 [d]
	14 060–14 200 [d]	280σ [d]	10	$\Gamma_2 \rightarrow \Gamma_{3,4}$	2540–2680 [d]
$^3H_6$	12 496	83π	30	$\Gamma_1 \rightarrow \Gamma_2$	4314
	12 426	3σ	10	$\Gamma_2 \rightarrow \Gamma_2$ (MD)	4314
	12 346	1000σ	10	$\Gamma_2 \rightarrow \Gamma_{3,4}$	4394
	12 346	21π	10	$\Gamma_2 \rightarrow \Gamma_{3,4}$ (MD)	4394
	12 286	139σ	10	$\Gamma_2 \rightarrow \Gamma_{3,4}$	4454
	12 254	284π	10	$\Gamma_2 \rightarrow \Gamma_1$	4486
	11 833	190σ	10	$\Gamma_2 \rightarrow \Gamma_{3,4}$	4907
$^3F_2$	11 609	$>1000\pi$	80	$\Gamma_1 \rightarrow \Gamma_2$	5201
	11 589	732σ	80	$\Gamma_1 \rightarrow \Gamma_{3,4}$	5221
	11 539	68σ	10	$\Gamma_2 \rightarrow \Gamma_2$ (MD)	5201
	11 519	1000σ	10	$\Gamma_2 \rightarrow \Gamma_{3,4}$	5221
	11 519	100π	10	$\Gamma_2 \rightarrow \Gamma_{3,4}$ (MD)	5221
$^3F_3$	10 329	4σ	30	$\Gamma_1 \rightarrow \Gamma_{3,4}$	6481
	10 289	67π	30	$\Gamma_1 \rightarrow \Gamma_2$	6521
	10 259	753σ	10	$\Gamma_2 \rightarrow \Gamma_{3,4}$	6481
	10 259	13π	10	$\Gamma_2 \rightarrow \Gamma_{3,4}$ (MD)	6481
	10 219	35σ	10	$\Gamma_2 \rightarrow \Gamma_2$ (MD)	6521
	10 154	1000π	10	$\Gamma_2 \rightarrow \Gamma_1$	6586
	10 139	13σ	30	$\Gamma_1 \rightarrow \Gamma_{3,4}$	6671
	10 124	π	80	$\Gamma_1 \rightarrow \Gamma_2$	6686
	10 069	442σ	10	$\Gamma_2 \rightarrow \Gamma_{3,4}$	6671
	10 069	22π	10	$\Gamma_2 \rightarrow \Gamma_{3,4}$ (MD)	6671
$^3F_4$	9 868	10σ	30	$\Gamma_1 \rightarrow \Gamma_{3,4}$	6942
	9 827	π [e]	30	$\Gamma_1 \rightarrow \Gamma_2$	6983
	9 820	148π	10	$\Gamma_2 \rightarrow \Gamma_1$	6920
	9 798	182σ	10	$\Gamma_2 \rightarrow \Gamma_{3,4}$	6942
	9 694	π	80	$\Gamma_1 \rightarrow \Gamma_2$	7116
	9 668	9σ	30	$\Gamma_1 \rightarrow \Gamma_{3,4}$	7142
	9 635	611π	10	$\Gamma_2 \rightarrow \Gamma_1$	7105
	9 598	1000σ	10	$\Gamma_2 \rightarrow \Gamma_{3,4}$	7142
	9 518	371π	10	$\Gamma_2 \rightarrow \Gamma_1$	7220

[a] MD: magnetic dipole.
[b] Intensity is uncertain because of vibronic structure in spectrum.
[c] May represent two Γ_1 levels which are predicted theoretically to be extremely close (see Table VII).
[d] Very broad structured band.
[e] Weak temperature-dependent shoulder.

TABLE VII. Experimental and theoretical energy levels of Pr^{3+} in $LiYF_4$. Theoretical levels were calculated using the parameters given by Eq. (10). The irreducible representations Γ_i are given for S_4 and D_{2d} symmetries. Calculated g values are given for $\Gamma_{3,4}$ levels (S_4 notation).

Multiplet	ν_E (expt) (cm^{-1})	ν_E (calc) (cm^{-1})	S_4	D_{2d}	$g_{\parallel}$
$^3H_4$	0	7	2	4	
	79	84	3,4	5	−3.600
	◦◦◦	217	1	1	
	220	218	1	2	
	496	487	3,4	5	0.170
	•••	512	1	1	
	◦◦◦	514	2	3	
$^3H_5$	2 253	2 255	1	2	
	2 272	2 264	3,4	5	1.149
	2 280	2 285	2	3	
	2 297	2 286	1	1	
	2 341	2 336	3,4	5	4.908
	2 549	2 567	2	4	
	◦◦◦[a]	2 588	1	2	
	◦◦•[a]	2 608	3,4	5	0.065
$^3H_6$	4 314	4 309	2	4	
	4 394	4 409	3,4	5	1.617
	◦◦•	4 430	1	1	
	◦◦◦	4 458	2	3	
	4 454	4 476	3,4	5	5.654
	4 486	4 511	1	2	
	4 557	4 558	2	4	
	◦◦◦	4 879	1	1	
	4 907	4 882	3,4	5	0.184
	4 945	4 926	2	3	
$^3F_2$	•••	5 159	1	1	
	5 201	5 235	2	4	
	5 221	5 218	3,4	5	0.789
	5 342	5 321	2	3	
$^3F_3$	6 481	6 478	3,4	5	−0.433
	6 521	6 526	2	4	
	6 586	6 562	1	2	
	6 671	6 673	3,4	5	−4.596
	6 686	6 717	2	3	
$^3F_4$	6 920	6 912	1	1	
	6 942	6 919	3,4	5	−2.310
	6 983	6 957	2	4	
	7 105	7 134	1	2	
	7 116	7 123	2	3	
	7 142	7 143	3,4	5	−1.226
	7 220	7 255	1	1	
$^1G_4$	9 699	9 715	1	1	
	9 832	9 815	3,4	5	−4.575
	9 930	9 931	2	4	
	10 011	10 021	2	3	
	10 112	10 170	3,4	5	0.228
	10 217	10 140	1	2	
	10 313	10 592	1	1	
$^1D_2$	16 740	16 868	2	3	
	16 810	16 817	1	1	
	17 083	17 080	3,4	5	2.121
	17 406	17 404	2	4	
$^3P_0$	20 860	20 860	1	1	
$^1I_6$	•••	21 083	2	3	
	•••	21 084	2	4	
	•••	21 401	3,4	5	3.225
	•••	21 414	1	1	

TABLE VII. *(Continued)*

Multiplet	ν_E (expt) (cm^{-1})	ν_E (calc) (cm^{-1})	S_4	D_{2d}	$g_{\|\|}$
	...	21 415	2	3	
$^3P_1$	...	21 443	3,4	5	0.736
	...	21 611	1	2	
$^1I_6$	...	21 622	3,4	5	7.514
	...	21 759	1	2	
	...	22 033	1	1	
	...	22 044	3,4	5	−2.279
	...	22 055	2	4	
$^3P_2$	22 498 [b]	22 508	1	1	
	22 645 [b]	22 636	3,4	5	2.663
	...	22 680	2	3	
	...	22 777	2	4	
$^1S_0$	...	48 831	1	1	

[a] Transitions to these levels were observed but the lines are very broad. Hence the energy levels (given in Tables V and VI) are not included here.

[b] This work. These energies are in agreement with those in Ref. 2.

rules. Evidence for magnetic dipole transitions was also found but these transitions were generally less intense than the electric dipole transitions.

A complete identification of the $^3P_0$ and $^1D_2$ energy levels was made from the absorption data in Table IV. These results are in basic agreement with Refs. 1 and 2, although our line positions agree more closely with those of Ref. 2. The energy levels of the $^1G_4$ multiplet were established completely from absorption data and from the $^3P_0$ fluorescence. A determination of the energy levels of the ^3H and ^3F states was made from $^3P_0$ and $^1D_2$ fluorescence data, summarized in Tables V and VI, respectively.

Experimental energy levels of Pr^{3+} in $LiYF_4$ are listed in Table VII for each multiplet studied. The irreducible representations are given in the table for both S_4 and D_{2d} site symmetries. Many low-intensity or missing π transitions can be explained by considering the Pr^{3+} ion to be in a S_4 symmetry site which is nearly D_{2d}. It can be seen from Tables I and II that π transitions between Γ_1 and Γ_2 states (S_4 notation) are allowed according to S_4 selection rules, but may be forbidden in D_{2d}. Table II shows that Γ_1 levels in S_4 notation correspond to either Γ_1 or Γ_2 levels in D_{2d}, while Γ_2 levels in S_4 correspond to either Γ_3 or Γ_4 in D_{2d}. According to D_{2d} selection rules $\Gamma_1 \leftrightarrow \Gamma_4$ and $\Gamma_2 \leftrightarrow \Gamma_3$ transitions are allowed (A) while $\Gamma_1 \leftrightarrow \Gamma_3$ and $\Gamma_2 \leftrightarrow \Gamma_4$ transitions are forbidden (F). Figures 1 and 2 contain partial energy-level diagrams for fluorescent transitions originating from the $^3P_0$ and $^1D_2$ levels, respectively. (These figures are not drawn to scale.) The D_{2d} representation (Γ_i) for each level is given to the right of the energy-level diagram. The D_{2d} selection rules and experimental observations are included for each transition.

The singlet $^3P_0$ level is Γ_1 for both S_4 and D_{2d} symmetries. The D_{2d} selection rules listed in Fig. 1 indicate that only half of the $\Gamma_1 \rightarrow \Gamma_2$ transitions (S_4 notation) in the $^3P_0$ fluorescence are allowed in D_{2d} symmetry. As shown in the figure strong emission lines were observed for all D_{2d} allowed transitions. For the most part, forbidden transitions either were not observed (lines c, k, and o) or were very weak (lines e, i, and n). The forbidden transitions a and g, which are comparable in intensity to the allowed transitions, are somewhat stronger than one might expect for forbidden transitions. Nevertheless, the use of D_{2d} selection rules is generally successful in explaining missing or weak lines in the $^3P_0$ fluorescence spectra.

Low-temperature fluorescence from the $^1D_2$ multiplet originates from the lowest $^1D_2$ level which is Γ_2 in S_4 notation or Γ_3 in D_{2d}. At elevated temperatures fluorescence is also observed from the next lowest $^1D_2$ level, which is Γ_1 in both S_4 and D_{2d} notation. The selection rules listed in Fig. 2 indicate that fewer than one-half of these transitions are allowed in D_{2d}. In the low-temperature fluorescence shown in Fig. 2, all allowed transitions were observed (lines c, g, o, s, u, and x). The peak intensity for line s is much lower than for other allowed transitions, but this line is extremely broad and the integrated intensity is actually quite high. Generally those D_{2d} forbidden transitions originating from the Γ_3 level either are not observed (lines k, m, q, v, and y) or are weak (line t). Theoretically line y is predicted to be very close to the observed line x and, being D_{2d} for-

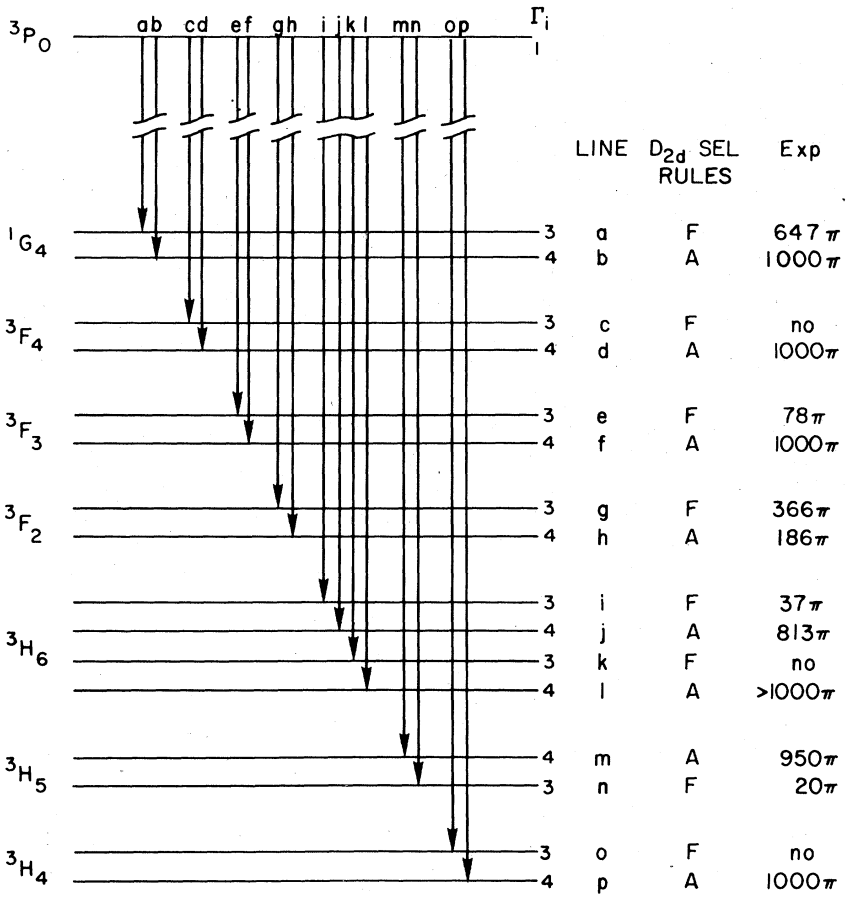

FIG. 1. Partial energy-level diagram (not to scale) showing $\Gamma_1 \rightarrow \Gamma_2$ transitions (S_4 notation) in the $^3P_0$ fluorescence. The D_{2d} representation for each level, as well as D_{2d} selection rules and experimental observations are listed to the right of the energy level diagram.

bidden, it is expected to be weaker than line x and should be difficult to detect. Hence line y may actually be present in the experimental spectrum as a weak line superimposed on line x. The forbidden D_{2d} lines a and e in the $^3F_4$ multiplet are weaker than the allowed line c in that multiplet. However they are stronger than one might expect for forbidden transitions. At higher temperatures, transitions originating from the $^1D_2$ Γ_1 level were also observed. At 80°K the allowed transition to the $^3F_2$ multiplet was observed while the forbidden one was not. For the $^3H_4$, $^3F_3$, and $^3F_4$ multiplets all allowed transitions were observed and forbidden ones absent in 30-°K spectra. The forbidden lines in the $^3F_3$ and $^3F_4$ fluorescence (lines b and f) were observed when the temperature was raised to 80°K. Finally the two forbidden transitions to the $^3H_6$ multiplet were not observed at 30°K. However, only one of the two allowed transitions was observed. The other allowed transition (line n) apparently is weak and could not be identified because of background vibronic structure in this region of the spectrum.

The use of D_{2d} selection rules as a rule of thumb to explain missing or weak π transitions has been successfully demonstrated here for $LiYF_4:Pr^{3+}$. With few exceptions π lines which were allowed in D_{2d} as well as in S_4 were observed and usually were quite strong. Those π lines not allowed in D_{2d} were usually missing or quite weak. Many of the smaller π lines not expected in D_{2d} can be accounted for by small nonzero values of the imaginary components of B_{64} and the odd-fold B_{kq}.

V. CALCULATIONS

In previous work[23,24] a rationale was given for factoring the B_{kq} of the triply ionized lanthanide ions in a given host according to

$$B_{kq} = \rho_k A_{kq}\,, \tag{9}$$

where ρ_k is a host independent term containing the electronic radial integrals and shielding factors, and the A_{kq} are impurity ion independent crystal field components obtained for a particular host by performing a lattice summation

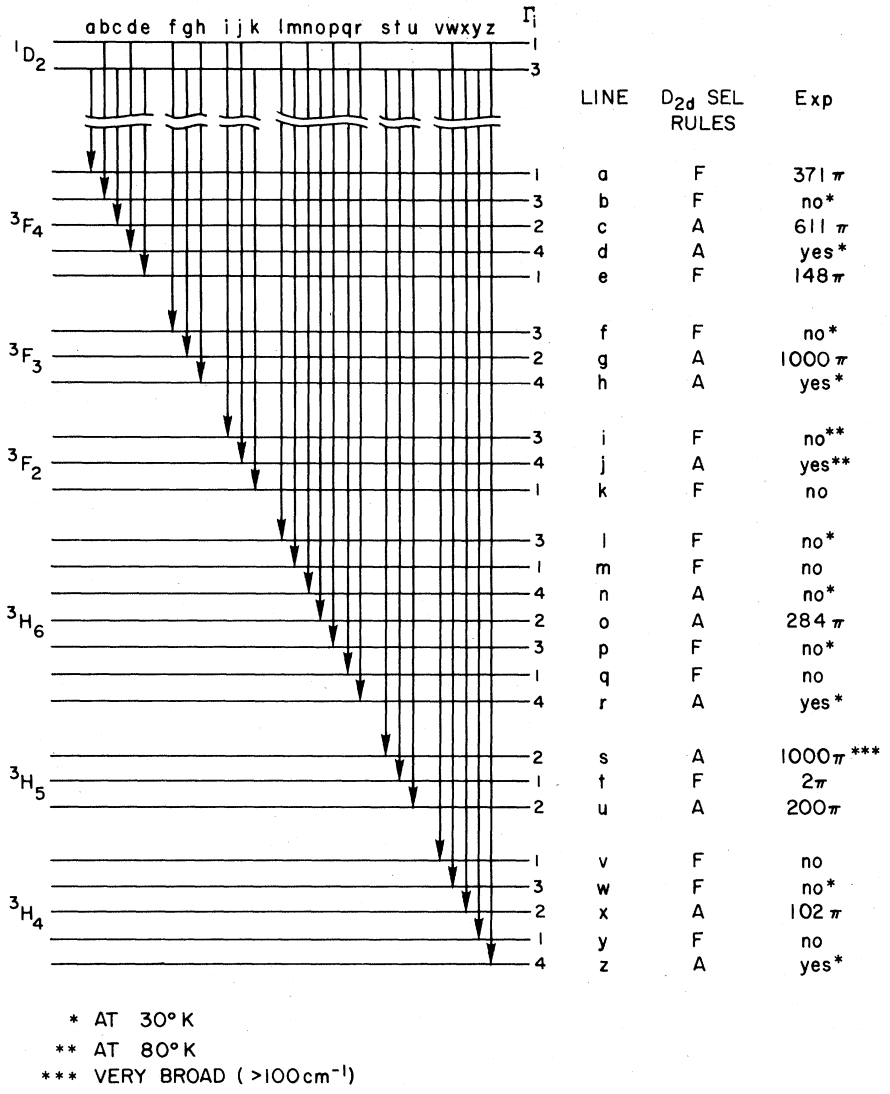

FIG. 2. Partial energy-level diagram (not to scale) showing $\Gamma_1 \rightarrow \Gamma_2$ and $\Gamma_2 \rightarrow \Gamma_1$ transitions (S_4 notation) in the $^1D_2$ fluorescence. The D_{2d} representation for each level, as well as D_{2d} selection rules and experimental observations are listed to the right of the energy-level diagram.

over the constituent ions. The ρ_k were given elsewhere[20] for the various rare earths so that approximate B_{kq} can be obtained for any of the lanthanide ions in a given host provided that B_{kq} have been determined for at least one of these ions in the host material. Preliminary values of the B_{kq} for $LiYF_4$:Pr^{3+} were obtained earlier[4] using the theoretical ρ_k to scale empirical B_{kq} for $LiYF_4$:Nd^{3+}. In the present work, this initial set of B_{kq} was varied in a least-squares calculation which used 36 energy levels in the multiplets $^3H_4$ through $^3P_0$. After using the calculated levels to aid in establishing an energy-level scheme for Pr^{3+} in $LiYF_4$, the parameters in Eq. (2) were varied until a least-rms value of 15.8 cm^{-1} between 41 calculated and experimental energy levels were obtained. The B_{kq} yielding this fit are in units of cm^{-1}:

$$B_{20} = 488.9 \pm 56, \quad B_{60} = -42 \pm 115,$$
$$B_{40} = -1043 \pm 140, \quad \mathrm{Re}B_{64} = 1213 \pm 58, \qquad (10)$$
$$B_{44} = 1242 \pm 93, \quad \mathrm{Im}B_{64} = 22.5 \pm 270,$$

where the ($\pm$) values correspond to the amount which each B_{kq} would have to change in order to produce a shift of 15.8 cm^{-1} in the energy level most sensitive to that particular B_{kq}. These values were determined from the calculated derivatives of the energy levels with respect to the B_{kq}.

The calculated energy levels for the ground configuration of Pr^{3+} in $LiYF_4$ are given together with the experimental levels in Table VII; both S_4 and D_{2d} notations for the corresponding levels

TABLE VIII. Phenomenological B_{kq} that fit the various terms of the $4f^2$ configuration for Pr^{3+} in $LiYF_4$. The units are cm^{-1}.

Term	B_{20}	B_{40}	B_{44}	B_{60}	Re B_{64}	Im B_{64}	rms deviation (cm^{-1})	No. levels
^3H	528	−1198	1318	−73	1245	99	10	17
^3H and ^3F	509	−1138	1268	−79	1212	−13	13	28
^1G	459	−253	925	−38	795	3	12	6
^3H through ^3P	489	−1043	1242	−42	1213	23	15.8	41

are given. The energy levels calculated for the ground term, ^3H, are in better agreement with the measurements than are those for the higher terms. Most of the calculated and measured ^3F levels are also consistent, but the calculations have the levels corresponding to 5201 and 5521 cm^{-1} inverted as are those at 7105 and 7116 cm^{-1}. Inversions also occur for the 10 112- and 10 217-cm^{-1} levels of $^1G_4$ and the 16 740- and 16 810-cm^{-1} levels of $^1D_2$. In addition, the calculated splitting of the $^1G_4$ multiplet was about 900 cm^{-1} whereas the measured splitting is 614 cm^{-1}. For that reason only the lower three energy levels of $^1G_4$ were used to obtain the best-fit parameters given by Eq. (10). The 16 740-cm^{-1} energy level of $^1D_2$ was also left out of the calculation to determine the B_{kq} given in Eq. (10).

A check was next made to see whether the $^1G_4$ energy levels could be fit separately since, for this multiplet, the predicted splitting overestimates the measured splitting by 50%. An rms deviation of 12 cm^{-1} resulted between six calculated and measured $^1G_4$ energy levels. However, the energy levels for the other multiplets calculated with the $^1G_4$ B_{kq} were not in agreement with the measurements. Similar calculations were made for the ^3H and ^3F multiplets, and the results are given in Table VIII. Since the higher-energy levels[25] mix more strongly with the next-higher electron configurations, the ground-configuration wave functions might be expected to describe the ^3H and ^3F levels better than the ^1G, ^1D, and ^3P levels. Hence the better agreement between calculated and measured ^3H levels, for example, might be expected. In addition, the calculated $g_{\parallel}$ factors for the double $\Gamma_{3,4}$ levels, which are listed in Table VII, require accurate wave functions and may be expected to be better for the lower-lying levels partly because of configuration mixing.

The even-fold B_{kq} for Pr^{3+} in $LiYF_4$, given in Eq. (10), are compared in Table IX with values obtained for Nd^{3+}, Ho^{3+}, Er^{3+}, and Tm^{3+} in $LiYF_4$ using the same theoretical model. As shown in the table, the magnitude of B_{kq} tends to decrease with increasing atomic number across the lanthanide series, in qualitative agreement with theoretical predictions.[20,24] Quantitatively, however, the phenomenological B_{kq} for $LiYF_4$ do not vary precisely as predicted by Eq. (9) with the ρ_k's calculated in Ref. 4. It has been suggested[24] that the agreement could be improved by incorporating effects such as wave functions overlap in the calculation of ρ_k. Another possible

TABLE IX. Crystal-field parameters for triply ionized rare earths in $LiYF_4$. The units are cm^{-1}. All ions are analyzed using the same method.

	Pr [a]	Nd [b]	Ho [c]	Er [b]	Tm [d]
B_{20}	489	441	410	400	333
B_{40}	−1043	−906	−615	−692	−648
B_{44}	1242	1114	819	925	876
B_{60}	−42	−26	−28	−21	−141
Re B_{64}	1213	1072	677	610	623
Im B_{64}	23	21	33	149	3
rms deviation (cm^{-1})	15.8	3.5	2.8	4.1	7.5
No. levels in fit	41	26	66	26	44

[a] This work.
[b] Reference 4.
[c] Reference 5.
[d] R. P. Leavitt refit the experimental levels reported in Ref. 6 using the method described in Sec. II A (private communication).

reason for the discrepancy is the experimental uncertainty in B_{kq}. The uncertainty limits given in Eq. (10) for Pr^{3+} illustrate that some of the energy levels are relatively insensitive to B_{kq}. Consequently somewhat different B_{kq} may be used without singnificantly changing the energy levels. In addition, the failure of the theory to accurately describe free ion levels may introduce further uncertainty in the B_{kq}'s.

Table IX also lists the number of levels used in the fit to obtain the B_{kq} and the rms deviation for each of the five ions. An rms deviation of 15.8 cm^{-1} among 41 calculated and measured energy levels for Pr^{3+} in $LiYF_4$ is somewhat larger than the rms values found for the other rare earths in $LiYF_4$. For approximately the same number of levels an rms deviation of 7.5 cm^{-1} is obtained for Tm^{3+}, which has a complementary electronic configuration to Pr^{3+} ($4f^{12}$ is treated like $4f^2$). In $LiYF_4$ the crystal-field splittings for Tm^{3+} are generally not as large as for Pr^{3+}. For example the splitting of the $^3F_3$ multiplet for Tm^{3+} is 85 cm^{-1} as compared to 205 cm^{-1} for Pr^{3+}. Such a comparison suggests that the Pr fit is comparable with the Tm fit. The calculated energy levels of $^1G_4$ and $^1D_2$ in Tm^{3+} are, as in Pr^{3+}, not in good agreement with experiment. For both of these ions, the energy levels used in the fitting procedures cover an energy range which includes all but the $^1S_0$ level.

Following the procedure described in Sec. II B, individual line intensities were calculated for absorption transitions from the ground state of the $^3H_4$ multiplet and for transitions between the fluorescing $^3P_0$ and $^1D_2$ levels and lower-lying energy levels. This is the first time that electric dipole transition strengths were calculated using odd-fold crystal field parameters determined *a priori* from a point-charge lattice sum. The calculated intensities were compared with experimental values. Table X contains a sample comparison for the $^3P_0 \rightarrow {}^3H_4$, $^3H_4 \rightarrow {}^1G_4$, and $^3H_4 \rightarrow {}^1D_2$ transitions. For convenience, relative intensities are compared, the strongest line in each set of transitions being normalized to 1000 for both experimental and calculated values.

Although the calculated intensities in Table X do not agree quantitatively with measured values, there is some qualitative agreement. This is illustrated by the $^3P_0 \rightarrow {}^3H_4$ fluorescence transitions. For a particular polarization (σ or π) the theory correctly predicts how the lines appear in order of increasing strength. The $^3P_0 \rightarrow {}^3H_4$ (79 cm^{-1}) σ transition is predicted to be two to three times stronger than the $^3P_0 \rightarrow {}^3H_4$ (496 cm^{-1}) σ line, in agreement with the data. For π polarization, the theory correctly predicts the $^3P_0 \rightarrow {}^3H_4$ (0 cm^{-1}) line to be much stronger than the $^3P_0 \rightarrow {}^3H_4$ (514 cm^{-1}) transition. However the relative magnitudes of calculated intensities between π and σ lines are reversed. Similar results are found for the $^3H_4 \rightarrow {}^1G_4$ transitions, where the order of the intensities of the π transitions are correctly predicted. Though the order of theoretical σ intensities does not agree with the data for $^3H_4 \rightarrow {}^1G_4$ transitions, both σ lines are predicted to be of nearly equal intensity, as are the experimental values. For $^3H_4 \rightarrow {}^1D_2$ absorption, theory and experiment give almost an exact fit. This surprising quantitative agreement is considered somewhat fortuitous. There are several probable reasons for the discrepancies noted between theory and experiment including the following: (a) The ground-configuration wave functions do not adequately describe levels of higher energy, such as the $^1G_4$ levels or those in the $^3P_0$ and $^1D_2$ fluorescing multiplets; (b) the odd-k A_{kq} are based on a point-charge lattice sum and are therefore approximate; (c) the Judd-Ofelt theory itself is an approximation. The above results are typical of what was observed for other transitions.

TABLE X. Calculated and measured intensities[a] of $^3P_0 \rightarrow {}^3H_4$, $^3H_4 \rightarrow {}^1G_4$, and $^3H_4 \rightarrow {}^1D_2$ transitions at 10 °K.

	Energy level (cm^{-1})	Relative intensity (Expt.)	Relative intensity (Calc.)
$^3P_0 \rightarrow {}^3H_4$	0	1000π	605π
	79	249σ	1000σ
	496	94σ	386σ
	[514]	···	53π
$^3H_4 \rightarrow {}^1G_4$	9 699	423π	1000π
	9 832	733σ	128σ
	10 112	1000σ	66σ
	10 217	10π	3π
	10 313	41π	600π
$^3H_4 \rightarrow {}^1D_2$	16 810	1000π	1000π
	17 083	797σ	784σ

[a] The strongest line of each set of transitions is normalized to 1000.

Other workers[25-28] have taken into account some of the interconfiguration effects on the $4f^2$ energy-level structure. Judd[28] recently approximated some of the effects of configuration mixing by introducing a two-electron operator which adds a correction to the even-fold crystal-field parameters. He improved the fit of the $^1D_2$ levels for Pr^{3+} in $LaCl_3$. His correction also is of the correct sign to improve the fit of the $^1D_2$ levels for Pr^{3+} in $LiYF_4$, but it would further spread the calculated $^1G_4$ splitting, which is already too

large. In a more complete treatment, Morrison *et al.*[25] introduced two-body operators which represent the excitation of a $4f$ electron to a higher-lying p or f orbital by means of the Coulomb interaction. This changed the even-fold crystal-field parameters by a small but significant amount. They improved the fit between the calculated and measured $^1D_2$ levels for Pr^{3+} in $LaCl_3$, and improved the overall fit of the $4f^2$ levels by about 3 cm^{-1}.

In this and in all previous[8] works, the intensities of transitions between Stark levels have been calculated using perturbation theory to include the effect of mixing of opposite parity configurations by the odd-fold crystal field. However, in Pr^{3+} the higher configurations of opposite parity lie relatively close to the ground configuration, and therefore the perturbation approach may not be adequate. This difficulty may be circumvented by diagonalizing the $4f^2$, $4f5d$, $4f6s$, and $4f5g$ configurations simultaneously, and fitting levels calculated in this way to experimental energy levels. The individual line intensities may then be calculated without resort to perturbation theory. Some of the discrepancies found in this work between calculated and experimental intensities for $LiYF_4$:Pr^{3+} might be resolved by including the effect of the odd-fold crystal-field interaction in this manner.

VI. CONCLUSIONS

Energy levels for the $4f^2$ ground configuration of Pr^{3+} in $LiYF_4$ were established from high-resolution absorption and fluorescence spectra. Energy-level assignments were made assuming electric dipole transition selection rules for S_4 site symmetry. The wide band gap of $LiYF_4$ enabled spectral measurements to be made for all terms in the ground configuration except for the $^1S_0$ singlet level. From these measurements 46 energy levels were established, including 44 in the lowest nine multiplets. Crystal-field parameters were determined by fitting 41 of these levels with an rms deviation of 15.8 cm^{-1}. These parameters were then used to obtain the remaining energy levels, yielding a complete energy-level scheme for the $4f^2$ configuration of Pr^{3+}. Agreement between calculated and experimental energy levels was found to be better for the lower terms than for higher terms. Even-k B_{kq} parameters for $LiYF_4$:Pr^{3+} were compared with values obtained for Nd^{3+}, Ho^{3+}, Er^{3+}, and Tm^{3+} using the same theoretical model. The magnitude of B_{kq} decreases with atomic number for the lanthanide series.

In the analysis of the experimental data, D_{2d} electric dipole selection rules were also considered in order to explain missing or weak transitions which are allowed in S_4. Generally, π lines which are allowed in D_{2d} as well as in S_4 were observed and were quite strong. Those π transitions allowed in S_4 but forbidden in D_{2d} were usually missing or quite weak. Hence the use of D_{2d} selection rules has been a useful rule of thumb in identifying energy levels and explaining weak or missing transitions in $LiYF_4$:Pr^{3+}.

Electric dipole transition strengths were determined using odd-fold crystal-field parameters calculated *a priori* from a lattice sum. The calculated intensities are in qualitative agreement with experiment. Generally, the theory predicts the correct order of intensities for transitions of a particular polarization. However predictions of the relative line strengths within a given polarization and the relative intensities between the two polarizations are unreliable.

Future work will focus on refinements to the crystal-field theory in order to improve predictions of energy levels and line strengths. Inclusion of configuration interaction using an approach similar to Morrison *et al.*[25] should remove some of the discrepancies in the energy-level calculation by improving the even B_{kq}. Explicit consideration of opposite parity configurations as described in this work will affect the odd B_{kq} and may improve the agreement between calculated and experimental intensities.

---

*Sponsored by the Office of Naval Research.

[1]H. P. Jenssen, U. S. National Technical Information Service, Springfield, Va., Report No. AD-731 742 (unpublished).

[2]H. H. Caspers and H. E. Rast, J. Lumin. 10, 347 (1975).

[3]M. R. Brown, K. G. Roots, and W. A. Shand, J. Phys. C 2, 593 (1969).

[4]D. E. Wortman, N. Karayianis, and C. A. Morrison, U. S. National Technical Information Service, Springfield, Va., Report No. AD-A033 902 (unpublished).

[5]N. Karayianis, D. E. Wortman, and H. P. Jenssen, J. Phys. Chem. Solids 37, 675 (1976).

[6]H. P. Jenssen, A. Linz, R. P. Leavitt, C. A. Morrison, and D. E. Wortman, Phys. Rev. B 11, 92 (1975).

[7]In calculating multiplet-to-multiplet intensities, using the Judd-Ofelt theory, the agreement with experiment is generally poorer for Pr^{3+} than for the other rare-earth ions. See J. A. Caird, U. S. National Technical Information Service, Springfield, Va., Report No. AD-914193 (unpublished); M. J. Weber, T. E. Varitimos,

and B. H. Matzinger, Raytheon Research Division Technical Memorandum (unpublished).

[8]Earlier intensity calculations were made by adjusting the odd-fold crystal-field parameters to fit experimental intensities. Such an approach cannot predict line intensities for arbitrary rare-earth ions or host crystals. Individual line intensities for various rare-earth ions have been calculated by J. D. Axe, Jr., J. Chem. Phys. 39, 1154 (1963); B. J. Becker, Phys. Status Solidi B 43, 583 (1971); C. Delsart and N. Pelletier-Allard, J. Phys. (Paris) 32, 507 (1971); J. Phys. C 6, 1277 (1973); P. Porcher and P. Caro, J. Chem. Phys. 68, 4176 (1978); J. Chem. Phys. 68, 4183 (1978). Many authors have reported multiplet-to-multiplet intensities for the various rare-earth ions. For the Pr^{3+} ion, see, W. T. Carnall, P. R. Fields, and B. G. Wybourne, J. Chem. Phys. 42, 3797 (1965); W. F. Krupke, Phys. Rev. 145, 325 (1966); M. J. Weber, J. Chem. Phys. 48, 4771 (1968); Phys. Rev. 171, 283 (1968). Multiplet-to-multiplet intensities for Nd^{3+}in $LiYF_4$ have been reported by T. S. Lomheim and L. G. DeShazer, Opt. Commun. 24, 89 (1978).

[9]L. Esterowitz, R. Allen, M. Kruer, F. Bartoli, L. S. Goldberg, H. P. Jenssen, A. Linz, and V. O. Nicolai, J. Appl. Phys. 48, 650 (1977).

[10]E. P. Chicklis, C. S. Naiman, R. C. Folweiler, D. R. Gabbe, H. P. Jenssen, and A. Linz, Appl. Phys. Lett. 19, 119 (1971).

[11]M. J. Weber, in *Handbook of Lasers*, edited by R. J. Presseley (Chemical Rubber, Cleveland, 1971).

[12]B. G. Wybourne, *Spectroscopic Properties of Rare Earths* (Wiley, New York, 1965).

[13]W. T. Carnall, P. R. Fields, and K. J. Rajnak, J. Chem. Phys. 49, 4424 (1968).

[14]The nonvanishing odd-fold parameters in S_4 are B_{32}, B_{52}, B_{72}, and B_{76}.

[15]B. R. Judd, Phys. Rev. 127, 750 (1962).

[16]G. S. Ofelt, J. Chem. Phys. 37, 511 (1962).

[17]E. U. Condon and G. H. Shortley, *The Theory of Atomic Spectra* (Cambridge University, Cambridge, England, 1959).

[18]P. Grossgut, thesis (Texas Christian University, 1971) (unpublished), available from University Microfilms, Ann Arbor, Mich., No. 72-07621.

[19]A. J. Freeman and R. E. Watson, Phys. Rev. 127, 2058 (1962).

[20]C. A. Morrison, N. Karayianis, and D. E. Wortman, U. S. National Technical Information Service, Springfield, Va., Report No. AD-A042 447 (unpublished).

[21]G. F. Koster, J. O. Dimmock, R. G. Wheeler, and H. Statz, *Properties of the Thirty-Two Point Groups* (MIT, Cambridge, Mass., 1963).

[22]The transition to D_{2d} symmetry may be performed in either of two ways: (a) by making B_{44} and B_{64} real, and making all the odd-k B_{kq} real, or (b) by making B_{44} and B_{64} real, and making all odd-k B_{kq} pure imaginary. The second scheme is usually the one chosen (see Ref. 21); it is related to the first by a rotation of 45° about the fourfold symmetry axis. In particular the crystal-field parameters in the second scheme may be obtained from those in the first by changing the sign of B_{44} and B_{64}, multiplying B_{32}, B_{52}, and B_{72} by i, and multiplying B_{76} by $(-i)$. We have chosen the first scheme since it agrees with our convention of choosing $B_{44} > 0$.

[23]N. Karayianis and C. A. Morrison, U. S. National Technical Information Service, Springfield, Va., Report No. AD-A011 252 (unpublished).

[24]R. P. Leavitt, C. A. Morrison, and D. E. Wortman, U. S. National Technical Information Serivce, Springfield, Va. Report No. AD-A017 849 (unpublished).

[25]J. C. Morrison, P. R. Fields, and W. T. Carnall, Phys. Rev. B 2, 3526 (1970).

[26]E. Y. Wong, J. Chem. Phys. 38, 976 (1963).

[27]K. Rajnak, thesis (University of California, 1963) (unpublished), available from University Microfilms, Ann Arbor, Mich., No. 63-05545.

[28]B. R. Judd, Phys. Rev. Lett. 39, 242 (1977).